International Journal of Engineering & Technology, 7 (4) (2018) 4795-4800

International Journal of Engineering & Technology

Website: www.sciencepubco.com/index.php/IJET
doi: 10.14419/ijet. v7i4.24019
Research paper

Dynamic and hybrid phase shift controller for dual active bridge converter

S. Narasimha [1], S. Surender Reddy [2] *

[1] *Department of Electrical and Electronics Engineering, TKR College of Engineering & Technology, Hyderabad, India*
[2] *Department of Railroad and Electrical Engineering, Woosong University, Daejeon, Republic of Korea*
**Corresponding author E-mail: surender@wsu.ac.kr*

Abstract

This paper proposes a dynamic dual active bridge (DAB) converter and a hybrid phase shift control (HPSC) scheme for a (0.5-1) variation in the voltage conversion ratio. The proposed HPSC scheme is a combination of extended phase shift (EPS) and triple phase shift (TPS) modulations. It also provides a simple closed-form implementation for the primary and secondary-side phase-shift angles. During the light load operation of dynamic DAB converter, the TPS modulation is employed such that the practical zero voltage sequence operation can be extended to zero load. For heavy loads, the secondary-side phase-shift angle decreases to zero, hence the EPS modulation is applied. In this paper, the MATLAB Simulink software is used with an input voltage range of (200-400)V and then the output voltage wave forms are investigated for both EPS and TPS modulations for different operating modes of buck and boost operations.

Keywords: *Hybrid Phase Shift Control; Extended Phase Shift; Triple Phase Shift; Dual Active Bridge Converter; Buck and Boost Operations.*

1. Introduction

The single phase-shift modulation is simple and easy to implement, hence it is commonly employed in many applications. However, the soft-switching range is limited with single phase-shift (SPS) modulation, and the non-active power also termed as backflow power or reactive power is high as well. The enhanced phase-shift methods are generally termed as pulse width modulation plus phase-shift control [1]. To achieve the best performance of the dual active bridge (DAB) converter over a wide operating range, several modulation methods are combined and the hybrid phase-shift (HPS) schemes are introduced. When considering minimum inductor current for a short dead time interval, even larger parts of the theoretical zero voltage sequence (ZVS) region involve the incomplete commutation due to the parasitic output capacitance of MOSFETs, leads to reduced performance and efficiency [2]. However, most of the control schemes so far presented in the literature on DAB converter only considers the theoretical ZVS constraint, i.e., the inductor current at the switching instant should be of the right polarity (either positive or negative) [3].

In order to achieve practical ZVS of all switches, a commutation inductor is utilized by decreasing the magnetizing inductance or placing an external inductor between the two phase-leg midpoints in a full bridge, thereby, generating sufficient inductive current to charge and discharge the parasitic output capacitances. The additional commutation inductance current is uncontrolled, and processed by power MOSFETs [4]. An adaptive inductor is used as the main power transfer element such that the practical ZVS operation can be achieved at light loads and also the conduction losses are minimized at heavy loads. However, the voltage conversion ratio is limited to unity and the adaptive inductor increases the complexity of implementation. Recently, the variable-frequency phase-shift control tends to be focused and the soft-switching range is reduced. In general, the wide frequency variation increases the design complexity of passive components [5].

Reference [6] proposes a dual-bridge series resonant converter with dual tank to widen the soft-switching range and to improve the circuit performance. The design of a variable-voltage DC source using proportional and integral (PI) controller such as fuzzy logic controller (FLC) is proposed in [7]. Reference [8] presents advanced power control methods and new isolated bidirectional DC-DC topologies to improve the performance of isolated bidirectional converters. An overview of dual-active-bridge (DAB) isolated bidirectional dc-dc converter (IBDC) for high-frequency-link (HFL) power conversion systems (PCSs) is presented in [9]. An observer-based digital control system to manage active and reactive powers in a dual active bridge converter is proposed in [10]. A single sliding-mode controller (SMC) for charger/discharger DC/DC converter to provide a stable DC bus voltage in any operation condition is proposed in [11]. A novel method for the control of a buck-boost DC-DC converter with variable input voltage based on sliding mode control technique is proposed in [12].

The HPS control scheme is a combination of EPS and TPS modulations, and it provides a very simple closed form implementation for the primary and secondary side phase shift angles. With the help of MATLAB Simulink software, the output voltage wave forms are investigated for the characteristic table feedback control closed loop operation. By using 1D look up table, the proposed DAB converter provides constant 400V for any given input voltage (200-400)V and the ripple factor has been reduced to from 0.8% to 0.5%.

The rest of this paper is organized as follows: Section 2 presents the description of dual active bridge (DAB) converters. The description of proposed circuit topology is presented in Section 3. Simulation results and discussion is presented in Section 4. Finally, the conclusions are presented in Section 5.

2. Dual active bridge (DAB) converters

The working principle and different phase shift control techniques applied to DAB converters is described in this section. The proposed circuit diagram of DAB consists of two inductors and the derivation process has been explained here. The single-phase full converters with inductive loads permit solely a two-quadrant operation. Suppose, if two of those full converters area unit area are connected back to back, as shown in Figure 1, then the load current flow gets reversed. This system provides a four-quadrant operation and it is termed a dual converter. Dual converters are normally used in high-power variable-speed drives. If $\propto_1$and $\propto_2$ are the delay angles of converters 1 and 2, respectively, the corresponding average output voltages are V_{dc1} and V_{dc2}. The delay associate angles area unit controlled such that one device operates as a rectifier and another one operates as an inverter. However, each converter turns out constant average output voltage. The average output voltage of DAB converter are given by [13],

$$V_{dc1} = \frac{2V_m}{\pi}\cos\alpha_1 \quad (1)$$

$$V_{dc2} = \frac{2V_m}{\pi}\cos\alpha_2 \quad (2)$$

As mentioned earlier, one converter is rectifying and the other one is inverting, hence $V_{dc1} = -V_{dc2}$ or $\cos\alpha_2 = \cos\alpha_1 = \cos(\pi - \alpha_1)$. Therefore [14],

$$\alpha_2 = \pi - \alpha_1 \quad (3)$$

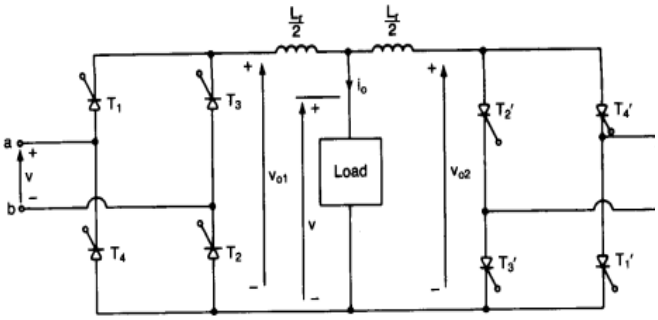

Fig. 1: Dual Active Bridge (DAB) Converter.

Control strategy is one of the important research directions for dual active bridge (DAB) isolated bidirectional dc-dc converter (IBDC). For improved topologies and variant, the control methods may be different. The reader may refer references [15]-[17] for different phase shift control techniques such as Single phase shift (SPS) Control, Extended phase shift (EPS) Control, Triple phase shift (TPS) Control, Hybrid phase shift (HPS) Modulation for dual active bridge (DAB) converters. In those references, the modulation description of both EPS and TPS modulations, their operating principles, equivalent circuits and idealized operating waveforms in different modes with soft switching characteristics has been presented.

As mentioned earlier, the major objective of this paper is to propose a modified DAB converter and a simple HPS control scheme. The HPS control scheme is a combination of EPS and TPS modulations, and it provides a very simple closed-form implementation for the primary and secondary-side phase-shift angles. When this modified DAB converter operates at light loads, the TPS modulation is employed such that the practical zero voltage sequence (ZVS) operation can be extended to zero load. As the load gets heavy enough, the secondary-side phase-shift angle decreases to zero, and the EPS modulation is applied to decrease the RMS current and conduction losses. Therefore, the proposed converter can operate efficiently over full operating range. Therefore, complete soft switching operation within a short dead time interval can be a direct optimization objective for DAB converters operating at high voltage and high frequency.

3. Proposed circuit topology

In this paper, a center tapped transformer (CTT) based DAB converter is proposed, by inserting a small inductor (L_s) between the transformer center tap and the mid-point of split output capacitors (C'_{s1} and C'_{s2}) in the conventional DAB converter topology. Here, the two-inductor CTT based DAB converter is used and it is shown in Figure 2(a). The turns ratio of CTT is $N_1{:}N_2 = N_1{:}N_3{=}n$. A T-type and a Δ-type primary-referred equivalent circuits of modified DAB converter are derived with the equivalent transformation of transformer and impedance. The magnetizing inductance (L_m) of CTT is neglected in this analysis and transformation, due to the fact that $L_m$is larger than the phase-shift inductors [18]. The CTT associated with two phase-shift inductors driven by three ac voltages are u_1, u'_2 and u'_3. CTT-based ac equivalent can be directly derived, as shown in Figure 2(a). By replacing the phase-shift inductor L'_s with two equal inductors (L'_2 and L'_3) connected in series with the secondary windings, the CTT-based ac equivalent circuit with three phase-shift inductors are derived and shown in Figure 2(b). The values of the three inductors that are used in this model are expressed as [19-20],

$$L_1 = L_p - L'_s \quad (4)$$

$$L'_2 = 2L'_s \quad (5)$$

$$L'_3 = 2L'_s \quad (6)$$

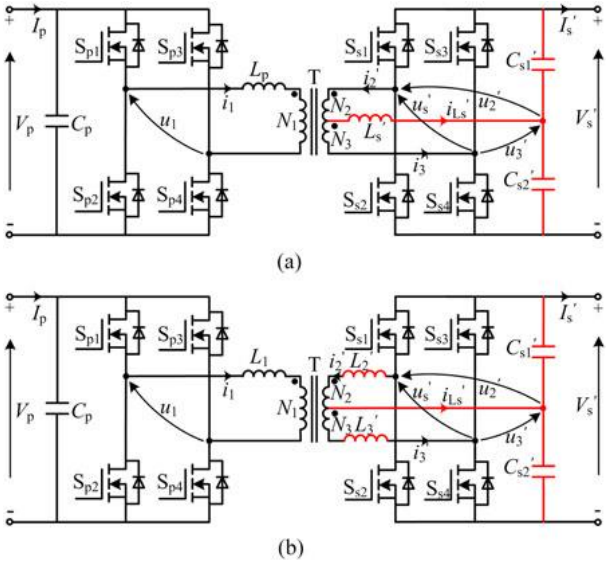

Fig. 2: Proposed CTT Based DAB Converter Topologies with (A) Two Inductors and (B) Three Inductors.

3.1. EPS modulation

The gate drive orders of switches and definition of two phase-shift angles are illustrated in Figure 3, where $u_s{=}u_2{+}u_3{=}\ 2u_T$, and u_T represents the ac voltage applied to the transformer magnetizing inductance. Ignoring the dead time, the upper and lower switches in each switching leg are determined complementarily with a duty cycle of 0.5. The two primary-side switching legs are $\emptyset_p$ out of phase, the two secondary-side switching legs are driven synchronously. With the EPS control, u_1 is characterized as an ac rectangular wave with amplitude V_p, and both u_2 and u_3 are ac square waves with the same amplitude V_s ($V_s{=}\ nV'_s$) [21].

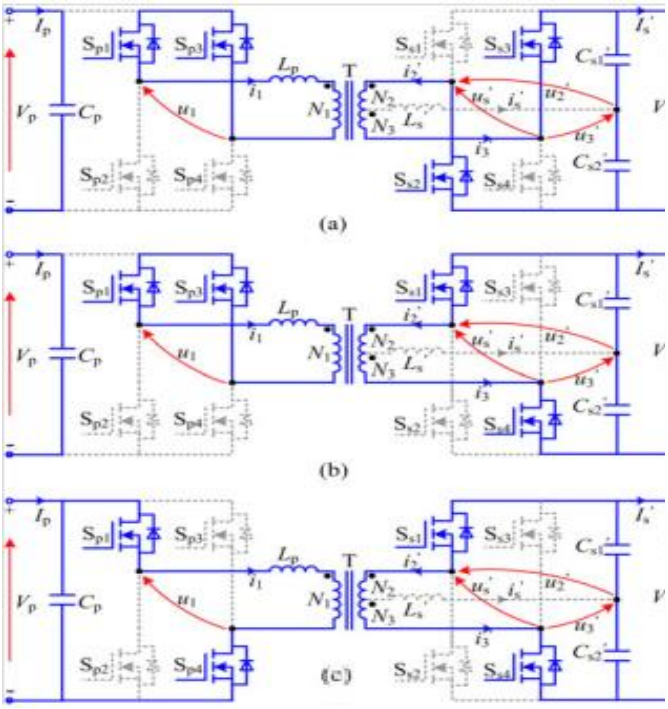

Fig. 3: Equivalent Circuits of Modified DAB Converter with EPS Control.

Mode 1 operation is considered as an example to explore the operation of modified DAB converter with the EPS control, and due to the symmetry, only three stages over the half switching are described. As mentioned earlier, three inductor currents i_1, i_2, and i_3 (in Figure 2(a)) can be derived with the superposition of the three decoupled currents i_{12}, i_{23}, and i_{31}which are determined by the voltages across three equivalent inductors L_{12}, L_{23}, and L_{31}. Since the two equivalent ac voltage sources u_2 and u_3 are synchronous always in the EPS control, the voltage across L_{23} is zero [22]. Therefore, I (θ) equals 0 as well, which means that no current flows through the inserted secondary-side inductor in EPS control [23].

3.2. Characteristic table closed loop feedback control

By using characteristic table closed loop feedback control, the output voltage will be 400V for any given input voltage of (200-400) V. This method reduces the ripple factor. To control output voltage with input voltage a tabular form is taken. The n-D Lookup Table represents function in N factors, and it is represented by [24],

$$y = F(x_1, x_2, x_3, \dots, x_N) \quad (7)$$

Where the capacity F can be exact. The maps contributions to an output by turning upward or introducing a table of qualities characterize with parameters. In the block, the primary information recognizes the principal measurement break points, the second information distinguishes the second measurement breakpoint. For interpolation and linear modes, the parameters should use the equal floating type such as breakpoints, output, and fraction.
Determine whether to enter information as breakpoints or as parameters that create uniformly spaced breakpoints. To expressly indicate the breakpoint information, set this parameter to explicit value and enter breakpoint information in box [25]. The block computes the quantity of points to produce from the table information the main point in your equitably separated breakpoint information. This parameter is accessible when breakpoints determination is set to even spacing. The dispersing between points in your equally separated breakpoint information. This parameter is accessible when breakpoints detail is set to even spacing. The breakpoint information expressly or as equitably dispersed breakpoints [26].
In the event that you set breakpoints determination to even dividing, enter the parameters first point and spacing in each breakpoints column to produce uniformly breakpoints in the particular measurement. This table information decides the quantity of equitably divided points. The breakpoints particular to explicit value, enter the breakpoint set that relates to each measurement of table information in each breakpoints row. For each measurement, indicate breakpoints as a 1-by-n or n-by-1 vector whose esteems are entirely monotonically expanding [27].

4. Results and discussion

In this paper, EPS and TPS modulations are applied and the IBDC operates in buck or boost operations. In this paper, four modes of operations are performed. For each mode of operation, MATLAB simulation circuit, output voltage and power waveforms are provided. In Mode 1 operation, buck operation wave forms are presented. In Mode 2 and 3 operations, boost operation wave forms are presented. In Mode 4, again buck operation wave forms are presented [28]. The input pulses given to the MOSFET switches for each mode of operation are presented in this paper. The characteristic table closed loop control method has been used for further enhancement in operation. The closed loop MATLAB circuit and its simulation output waveforms are described. The comparison of voltage wave forms with and without closed loop has been provided for further reference.

4.1. EPS control method

By using the EPS control method, Mode 1 operation will give the buck operation. The Simulink model of proposed circuit topology for buck operation (i.e., Mode 1 operation) is depicted in Figure 4. For the input of 200V, the output voltage has been step downed to 187V and the output power is 220W.

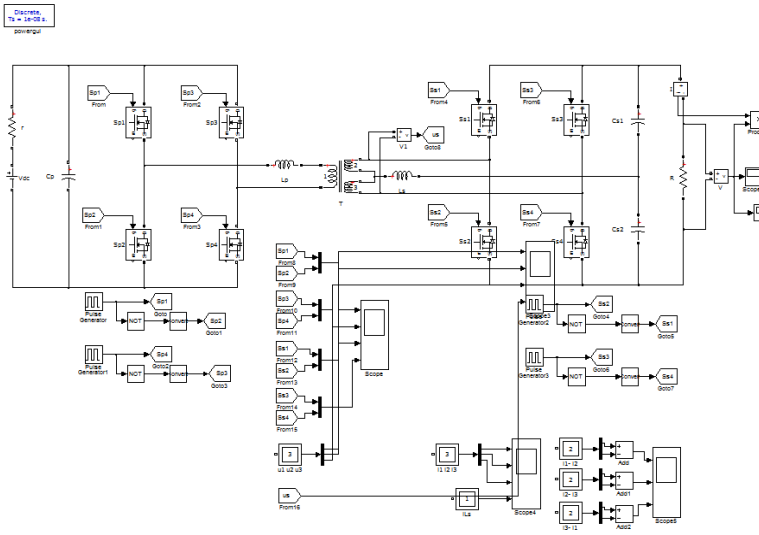

Fig. 4: Simulink Model of Proposed Topology for Buck Operation.

Figure 5 depicts the switching pulses applied to the power electronic devices. Figure 6 depicts the output voltage in buck mode (i.e., Mode 1) operation. For the given input voltage of 200V, the output voltage is step down to 187V.

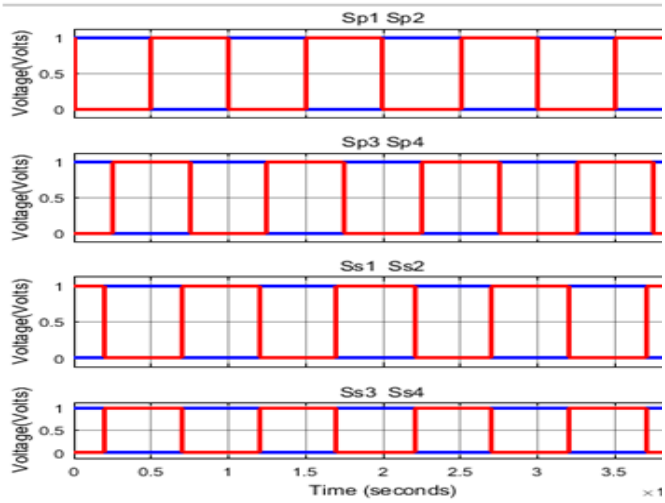

Fig. 5: Switching Pulses Applied to Power Electronic Devices.

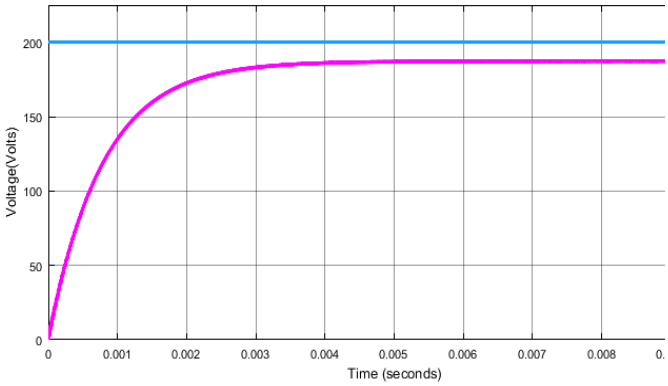

Fig. 6: Output Voltage of Converter with EPS Control (in Mode 1) for the Input Voltage of 200V.

Figure 7 shows the output power in buck mode operation EPS control. For the given input voltage of 200V, the obtained output power is 220W, and it can be observed in Figure 7.

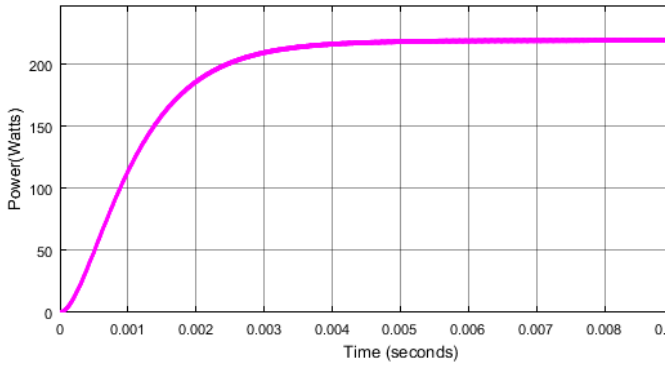

Fig. 7: Output Power of Converter with EPS Control (in Mode 1) for the Input Voltage of 200V.

4.2. TPS control method

The Simulink model of proposed topology for the boost operation is depicted in Figure 8. In Mode 2 operation, S_{s1} and S_{s4} are turned ON and this interval ends up with S_{p3} being switched OFF. In Mode 3 operation, S_{s1} is triggered ON and this interval ends up with S_{p1} being switched OFF. In TPS control method (i.e., Mode 2), the boost operation will give 543V output voltage for a given input voltage of 200V. Then, the output power is 1881W.

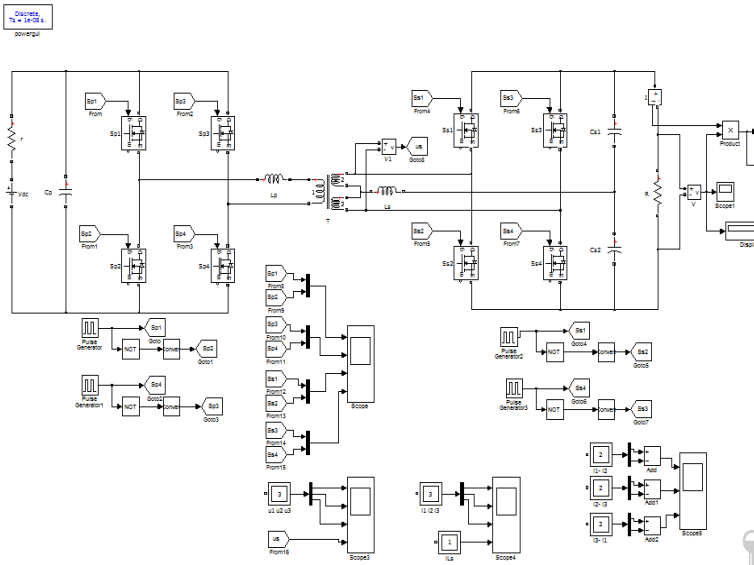

Fig. 8: Simulink Model of Proposed Topology for Boost Operation.

Figure 9 depicts the output voltage of the converter in TPS control boost operation. For the given input voltage of 200V, the obtained output voltage is 543V, and it can be seen from Figure 9. Figure 10 shows the output power of the converter in boost operation with TPS control. The obtained power output with 200V input voltage is 1846W.

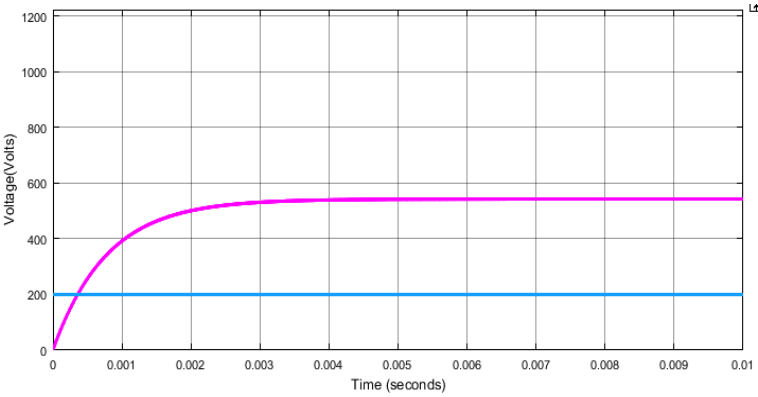

Fig. 9: Output Voltage of the Converter with TPS Control (in Mode 2) for the Input Voltage of 200V.

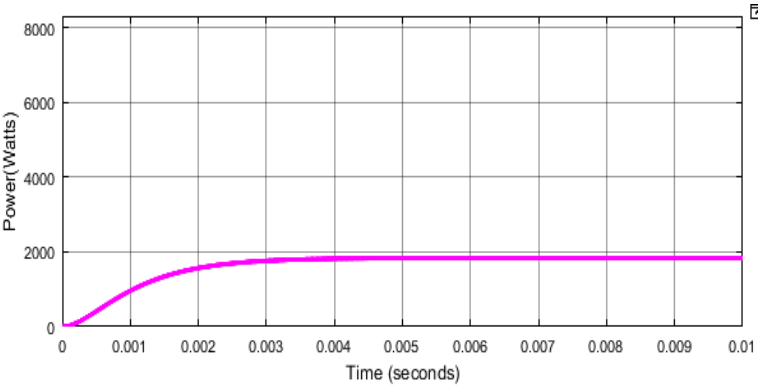

Fig. 10: Output Power of the Converter with TPS Control (in Mode 2) for the Input Voltage of 200V.

Figure 11 depicts the output voltage of the converter in boost operation (i.e., Mode 3). For the given input voltage of 200V, the obtained output voltage is 298V, and it can be observed from Figure 11. Figure 12 depicts the output power of the converter in boost operation (i.e., Mode 3). For the given input voltage of 200V, the obtained output power is 556W, and it can be observed from Figure 12.

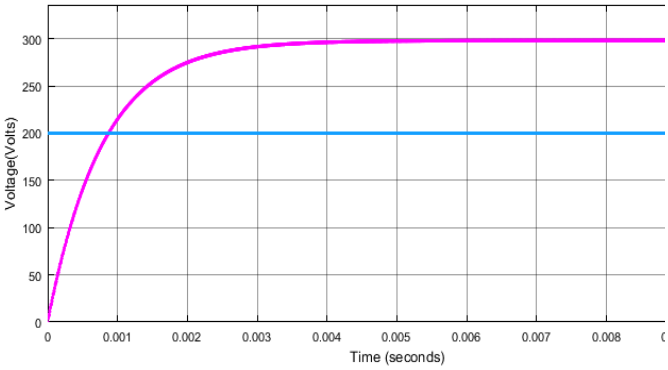

Fig. 11: Output Voltage of the Converter with TPS Control (I.E., Mode 3) for the Input Voltage of 200V.

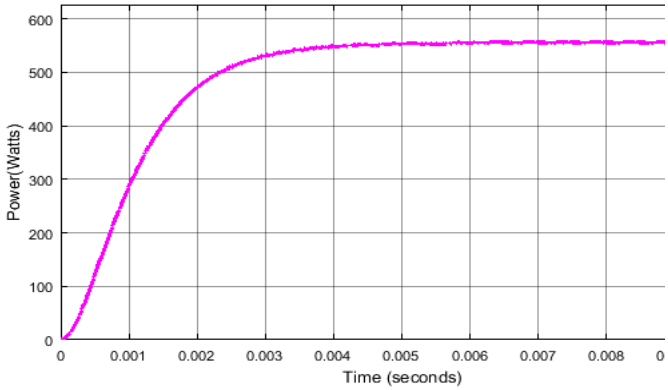

Fig. 12: Output Power of the Converter with TPS Control (I.E., Mode 3) for the Input Voltage of 200V.

Figure 13 depicts the output voltage of the converter in buck operation (i.e., Mode 4). For the given input voltage of 200V, the obtained output voltage is 77V. Figure 14 depicts the output power of the converter in buck operation (i.e., Mode 4). For the given input voltage of 200V, the obtained power output is 37W, and this can be observed from Figure 14.

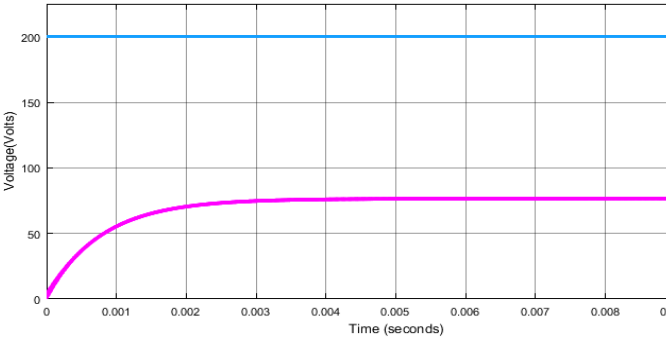

Fig. 13: Output Voltage of the Converter (I.E., Mode 4) for the Given Input Voltage of 200V.

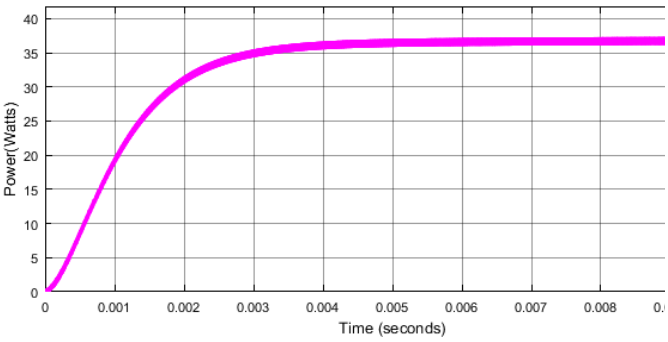

Fig. 14: Output Power of the Converter (I.E., Mode 4) for the Input Voltage of 200V.

4.3. Comparison of results

The output voltage waveforms without closed loop feedback and with closed loop feedback control of characteristic table method are compared in this section. The ripple factor has been reduced by using the feedback control. Figure 15 depicts the comparison of output voltage with and without the feedback control.

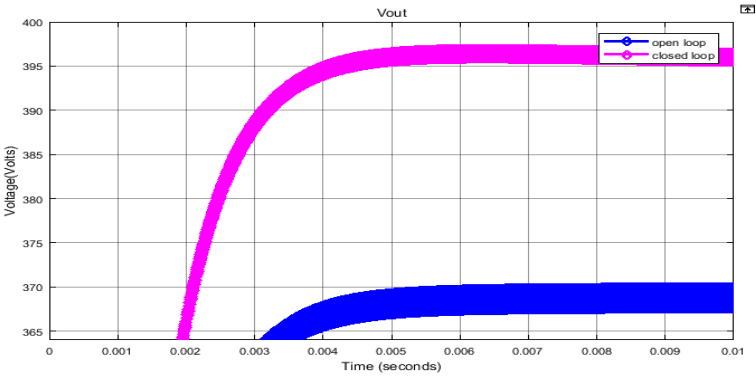

Fig. 15: Comparison of Output Voltage Waveforms for with and Without the Feedback Control.

Ripple factor without feedback is calculated as,

$$Ripple\ Factor = \frac{370-367}{370} * 100 = 0.8\% \quad (8)$$

Ripple factor with characteristic table closed loop feedback control is calculated as,

$$Ripple\ Factor = \frac{397-395}{397} * 100 = 0.5\% \quad (9)$$

From the above equations (8) and (9), it is clear that the ripple factor without feedback is 0.8% and the with feedback is 0.5%. From this, it can be observed that the ripple factor has been reduced significantly with characteristic table closed loop feedback control.

5. Conclusions

The hybrid phase shift (HPS) control scheme is a combination of extended phase shift (EPS) and triple phase shift (TPS) modulations, and it provides a very simple closed form implementation for the primary and secondary side phase shift angles. By applying EPS and TPS modulations the isolated bidirectional dc-dc converter (IBDC) operates in both buck or boost operation. Depending on the application, by changing the phase shift angles, buck or boost operations can be achieved. With the help of MATLAB Simulink software, for input voltages of (200-400) V, the output voltage wave forms have been investigated for both EPS and TPS modulations for different operating modes of buck and boost operations. The characteristic table feedback control method has been used for the closed loop operation.

Acknowledgments

This research work has been carried out based on the support of "TKR College of Engineering & Technology, India" and "Woosong University's Academic Research Funding - 2019".

References

[1] X. Sun, Y. Shen, W. Li, B. Wang, L. Wang, X. Li, Center-tapped transformer based bidirectional dc-dc converter with wide input

voltage range, IEEE Energy Conversion Congress and Exposition (ECCE), Montreal, QC, 2015, pp. 5910-5917.
[2] Available. [Online]. https://www.ieee.li/pdf/viewgraphs/bidirectional_dc_dc_converter_systems.pdf
[3] S. Zeljkovic, T. Reiter, D. Gerling, Single-stage reconfigurable DC/DC converter for wide input voltage range operation in HEVs, International Power Electronics Conference (IPEC-Hiroshima 2014 - ECCE ASIA), Hiroshima, 2014, pp. 774-781.
[4] X. Sun, X. Wu, Y. Shen, X. Li, Z. Lu, A Current-Fed Isolated Bidirectional DC–DC Converter, IEEE Transactions on Power Electronics, vol. 32, no. 9, pp. 6882-6895, Sept. 2017. https://doi.org/10.1109/TPEL.2016.2623306.
[5] N. Leena, B.D. Raj, R. Gunabalan, Computer-based laboratory teaching tools: An overview of LabVIEW and MATLAB, IEEE International Conference on Engineering Education: Innovative Practices and Future Trends (AICERA), Kottayam, 2012, pp. 1-6. https://doi.org/10.1109/AICERA.2012.6306686.
[6] J. Wu, Y. Li, X. Sun, F. Liu, A New Dual-Bridge Series Resonant DC–DC Converter With Dual Tank, IEEE Transactions on Power Electronics, vol. 33, no. 5, pp. 3884-3897, May 2018. https://doi.org/10.1109/TPEL.2017.2723640.
[7] C.H. Cheng, P.J. Cheng, M.T. Wu, Fuzzy logic design of self-tuning switching power supply, Expert Systems with Applications, vol. 37, no. 4, pp. 2929-2936, Apr. 2010. https://doi.org/10.1016/j.eswa.2009.09.043.
[8] D. Sha, G. Xu, High-Frequency Isolated Bidirectional Dual Active Bridge DC–DC Converters with Wide Voltage Gain, CPSS Power Electronics Series, Springer Nature, 2019. https://doi.org/10.1007/978-981-13-0259-6.
[9] B. Zhao, Q. Song, W. Liu, Y. Sun, Overview of Dual-Active-Bridge Isolated Bidirectional DC–DC Converter for High-Frequency-Link Power-Conversion System, IEEE Transactions on Power Electronics, vol. 29, no. 8, Aug. 2014. https://doi.org/10.1109/TPEL.2013.2289913.
[10] D.D. Nguyen, T.N. Duc, G. Fujita, An observer-based digital control system for individually management of active and reactive power of dual-active-bridge DC/DC converter, Journal of International Council on Electrical Engineering, vol. 7, no. 1, pp. 234-241, Sept. 2017. https://doi.org/10.1080/22348972.2017.1369925.
[11] S.I.S. Garcés, D.G. Montoya, C.A. Ramos-Paja, Sliding-Mode Control of a Charger/Discharger DC/DC Converter for DC-Bus Regulation in Renewable Power Systems, Energies, vol. 9, pp. 1-27, 2016.
[12] S.V. Drakunov, M. Reyhanoglu, B. Singh, Sliding Mode Control of DC-DC Power Converters, IFAC Proceedings Volumes, vol. 42, no. 19, pp. 237-242, 2009.
[13] H. Wen, W. Xiao, B. Su, Non-active Power Loss Minimization in a Bidirectional Isolated DC–DC Converter for Distributed Power Systems, IEEE Transactions on Industrial Electronics, vol. 61, no. 12, pp. 6822-6831, Dec. 2014. https://doi.org/10.1109/TIE.2014.2316229.
[14] M.S. Patil, S.P.Patil, D.N. Kyatanavar, Reversible DC Drive using MOSFET Chopper - A Laboratory Model Development for Undergraduate Students, vol. 50, no. 2, pp. 65-72, 2009.
[15] A. Tong, L. Hang, G. Li, X. Jiang, S. Gao, Modeling and Analysis of a Dual-Active-Bridge-Isolated Bidirectional DC/DC Converter to Minimize RMS Current With Whole Operating Range, IEEE Transactions on Power Electronics, vol. 33, no. 6, pp. 5302-5316, Jun. 2018 https://doi.org/10.1109/TPEL.2017.2692276.
[16] Y. Shen, X. Sun, W. Li, X. Wu, B. Wang, A Modified Dual Active Bridge Converter With Hybrid Phase-Shift Control for Wide Input Voltage Range, IEEE Transactions on Power Electronics, vol. 31, no. 10, pp. 6884-6900, Oct. 2016.
[17] W. Xu, N.H.L. Chan, S.W. Or, S.L. Ho, K.W. Chan, A New Control Method for a Bi-Directional Phase-Shift-Controlled DC-DC Converter with an Extended Load Range, Energies, vol. 10, pp. 1-17, 2017. https://doi.org/10.3390/en10101532.
[18] W. He, L. Jia, D. Li, J. Gao, A Kind of Self-tuning PID Controller and its Application on Marine Motion Control, Sixth International Conference on Intelligent Systems Design and Applications, Jinan, 2006, pp. 188-191. https://doi.org/10.1109/ISDA.2006.253830.
[19] B. Zhao, Q. Yu, Z. Leng, X. Chen, Switched Z-Source Isolated Bidirectional DC–DC Converter and Its Phase-Shifting Shoot-Through Bivariate Coordinated Control Strategy, IEEE Transactions on Industrial Electronics, vol. 59, no. 12, pp. 4657-4670, Dec. 2012. https://doi.org/10.1109/TIE.2011.2181136.
[20] P. Gananchchelvi, J. Yu, M.S. Pukish, Current trends in in-vehicle electrical engineering applications, IECON 2012 - 38th Annual Conference on IEEE Industrial Electronics Society, Montreal, QC, 2012, pp. 6268-6273.
[21] R.T. Naayagi, A.J. Forsyth, R. Shuttleworth, High-Power Bidirectional DC–DC Converter for Aerospace Applications, IEEE Transactions on Power Electronics, vol. 27, no. 11, pp. 4366-4379, Nov. 2012. https://doi.org/10.1109/TPEL.2012.2184771.
[22] Y. Xie, J. Sun, J.S. Freudenberg, Power Flow Characterization of a Bidirectional Galvanically Isolated High-Power DC/DC Converter Over a Wide Operating Range, IEEE Transactions on Power Electronics, vol. 25, no. 1, pp. 54-66, Jan. 2010. https://doi.org/10.1109/TPEL.2009.2024151.
[23] Z. Zhang, Z. Zhang, Y. Cao, Z. Wu, Q. Qian, S. Xie, Research on two current-fed isolated bidirectional DC/DC converters for the battery energy storage application, IEEE Southern Power Electronics Conference (SPEC), Puerto Varas, 2017, pp. 1-6.
[24] Z. Ling, H. Wang, K. Yan, J. Gan, Optimal Isolation Control of Three-Port Active Converters as a Combined Charger for Electric Vehicles, Energies, vol. 9, no. 9, pp. 1-15, 2016. https://doi.org/10.3390/en9090715.
[25] Z. Guo, K. Sun, Three-Level Bidirectional DC–DC Converter With an Auxiliary Inductor in Adaptive Working Mode for Full-Operation Zero-Voltage Switching, IEEE Transactions on Power Electronics, vol. 33, no. 10, pp. 8537-8552, Oct. 2018. https://doi.org/10.1109/TPEL.2017.2780853.
[26] M. Yaqoob, K. H. Loo, Y.M. Lai, A Four-Degree-Of-Freedom Modulation Strategy for Dual-Active-Bridge Series-Resonant Converter Designed for Total Loss Minimization, IEEE Transactions on Power Electronics, 2018.
[27] B. Zhao, Q. Song, W. Liu, Y. Zhao, Transient DC Bias and Current Impact Effects of High-Frequency-Isolated Bidirectional DC-DC Converter in Practice, IEEE Transactions on Power Electronics, vol. 31, no. 4, pp. 3203-3216, April 2016. https://doi.org/10.1109/TPEL.2015.2445831.
[28] T. Jiang, J. Zhang, X. Wu, K. Sheng, Y. Wang, A Bidirectional LLC Resonant Converter With Automatic Forward and Backward Mode Transition, IEEE Transactions on Power Electronics, vol. 30, no. 2, pp. 757-770, Feb. 2015. https://doi.org/10.1109/TPEL.2014.2307329.